Activation of existing surface crevasses has limited impact on grounding line flux of Antarctic Ice Streams

C. Gerli[1], S. Rosier[1], and G. H. Gudmundsson[1]

[1] Department of Geography and Environmental Sciences, Northumbria University, UK

Corresponding author: Cristina Gerli (cristina.gerli@northumbria.ac.uk)

Key Points:

- The instantaneous vertical propagation of pre-existing crevasses on major Antarctic ice shelves increases the mass flux of upstream glaciers.
- These flux changes are highly variable among ice shelves, with the largest effects occurring at the Filchner & Ronne and Ross Ice Shelves.
- Crevasses located near the main grounding lines are responsible for the majority of these flux changes.

Abstract

Recent studies have identified widespread vulnerable ice shelf regions in Antarctica which are both highly buttressed and susceptible to crevasse hydrofracturing, raising concern for potential crevasse driven ice-shelf collapse and future sea level rise. Here, we employ the finite element ice flow model, Úa, to investigate whether crevasses which have propagated through the entire ice column have a significant impact on upstream flow and quantify their contribution to sea level rise. We find a large variability in the response of ice shelves to this perturbation, with changes in grounding line flux as large as 155% for the Filchner-Ronne and 46% for the Ross, when compared to the present day. Crevasses located close to the grounding lines contribute most of this change. When compared to a second perturbation in which ice shelves are completely removed, however, the response is relatively small for all modelled ice shelves.

Plain Language Summary

In the last two decades, many ice shelves in Antarctica have disintegrated through the process of ice shelf thinning and calving. These processes reduce the resistance that ice shelves exert on upstream glaciers, increasing their mass flow and causing sea level to rise. In this work, we used a sophisticated model to quantify the maximum possible impact that crevasses developed throughout the ice shelf thickness would have on upstream glaciers' flow. We find that in all cases, fully propagated crevasses cause an increase in sea level rise, with Filchner & Ronne and Ross Ice Shelves having the largest contributions. The effect on upstream glaciers is dominated by crevasses located in grounded zone regions, where the ice shelf is thickest, and the provided back-stress is highest. However, when compared to other simulations in which all floating ice is disintegrated, the effect of crevasse propagation is minimal.

1 Introduction

Antarctic ice shelves are fundamental components of the cryosphere and key to predictions of global sea level rise. Their thinning and fracturing can reduce the buttressing stress exerted on the glaciers that flow into them, causing an increase in ice flux across their grounding lines (GL). The ability of ice shelves to modulate upstream grounding ice flow, has motivated studies on the impact of ice-shelf fracturing, thinning, and calving on mass loss of the Antarctic Ice Sheet (Fürst et al., 2016; Gudmundsson et al., 2019; Reese et al., 2018a; Sun et al., 2020). As several ice shelves in East Antarctica and in the Antarctic Peninsula are currently experiencing persistent Katabatic/ foehn winds that are increasing their surface temperatures and rising their melt flux, general concern has emerged among the scientific community regarding the development of more widespread surface meltwater on ice shelves. It has been suggested that this may in the future lead to increased crevasse hydrofracturing, which in turn might trigger unstable calving front retreat, irreversible ice loss, and sea level rise (DeConto & Pollard, 2016; Lai et al., 2020; Trusel et al., 2015).

To explore the susceptibility of ice shelves to crevasse hydrofracturing, a recent study used a deep convolutional neural network (DCNN) to map all fractural features on satellite imagery throughout Antarctica (Lai et al., 2020), and applied Linear Elastic Fracture Mechanics (LEFM) combined with the buttressing map product produced by Fürst et al., (2016), to obtain a vulnerability map. The authors suggested that 60 ± 10 % by area of all Antarctic ice shelves are highly buttressed regions which would be susceptible to crevasse propagation if inundated by water. Motivated by this work, we explore the scenario in which crevasses have propagated vertically through the entire ice shelf thickness and model the resulting impact on GL flux and sea level rise.

We are here primarily focused on quantifying the effect of widespread crevassing compared to a full ice-shelf disintegration. Rather than evolving the depth of individual crevasses with time, we consider the upper limit where all crevasses propagate instantaneously downwards through the whole ice-thickness. Hence, the goal of this work is to quantitatively analyse the *immediate* response on GL flux following the sudden propagation of all existing surface crevasses, as mapped by Lai et al., (2020), through the entire ice shelf thickness. We refer to this scenario hereafter as crevasse activation.

We include all major Antarctic ice shelves in our analysis, including all those previously estimated to have shown to exhibit a large increase in total ice discharge resulting from ice-shelf collapse (Fürst et al., 2016) and highest past sea level contribution (Rignot et al., 2019). To understand the scale of impact caused by fully vertically propagated crevasses in all vulnerable ice shelves regions, we compare the resulting change in GL flux to both 1) the currently observed GL flux for each basin, and 2) the change in GL flux when all floating ice shelves are fully disintegrated. We find that for certain ice shelves the impact is large compared to the former, but always small compared to the latter.

2. Methods

2.1 Overview

To assess the effect of crevasse activation on the Antarctic Ice Sheet we employ the finite element ice-flow model, Úa (Gudmundsson et al., 2012; Gudmundsson, 2013). The model solves the vertically integrated shallow shelf approximation (SSA) of MacAyeal, (1989) with an unstructured mesh, that allows refined resolution in complex areas, such as at the GL. Viscous ice deformation is described by the Glen–Steinemann flow law $\dot{\varepsilon}_e = A{\tau_e}^n$ where $\dot{\varepsilon}_e$ is the effective strain rate, A is the Arhenius ice rate factor, τ_e is the effective deviatoric stress, and n is the constant stress exponent, here set equal to 3. Basal motion is modelled using a Weertman sliding law $v_b = C{\tau_b}^m$ where v_b is the basal velocity, C is a sliding parameter, τ_b is the basal drag and m is the constant sliding exponent, here set equal to 3.

We modelled perturbations in GLs fluxes for both "crevassed" ice shelves, and for the case of full disintegration of all ice shelves. The impact of crevasses on flow was simulated by deactivating elements (i.e., entirely removing them from the mesh) that fall within a crevassed region.

We used several different criteria to determine if a given finite-element was within a crevassed region and should therefore be deactivated, providing upper and lower limits to the deactivated areas (further detail in Supplementary). Furthermore, we conducted extensive numerical-resolution convergence tests to ensure that our upper-limit estimates are numerically robust and concluded that (horizontal) mesh resolution on the order of 100m was sufficient for this purpose (see Supplementary, Section 3). In our "crevassed" simulations presented here we only deactivated elements within "vulnerable regions" of ice shelves, as categorized by Lai et al., (2020), where a full ice-thickness propagation of existing surface crevasses can be expected, provided sufficient surface meltwater production.

For each ice shelf, a domain was delineated following the drainage basins of Zwally et al., (2012) and using the 2008-2009 ice-front data from ALOS PALSAR and ENVISAT ASAR acquired during the International Polar Year, 2007-2009 (IPY) (Mouginot et al., 2017). At the grounded inflow boundaries of the domains, a zero-velocity condition was applied. To be able to further contextualize the resulting flux perturbations due to crevassing, we also then

modelled the more extreme scenario involving removal of all floating ice downstream of all grounding lines.

Initialization of the model

Simulations were performed with an initial ice thickness, surface elevation and bedrock topography taken from the Bedmachine Antarctica v2 dataset (Morlighem et al., 2020). The model was initialized by simultaneously inverting for both the basal slipperiness (C) and the ice rate factor (A) fields, by minimizing a cost function consisting of the sum of the misfit between modelled surface velocities and observed velocities (Landsat 8, Fahnestock et al., 2016), and a regularization term. We use a Tikhonov regularization term which consists of two parameters, γ_a and γ_s that penalize deviation of inferred parameter values (i.e., a total of 4 parameters, γ_a and γ_s applied to the ice rate factor A and to the basal slipperiness C independently) from their prior estimates and their spatial gradient. We selected the values of the regularisation parameters by performing an L-curve analysis (Supplementary, Section 2). The selected values of regularization parameters were in agreement with previous publications, using the same numerical model (Hill et al., 2018, 2020; Mitcham et al., 2021; Reese et al., 2018a; Rosier & Gudmundsson, 2018).

2.2 Numerical implementation of crevasse activation

To represent crevasses in the vulnerable regions of an ice shelf, we adopt the crevasse map product of Lai et al., (2020), which consists of a 125m gridded binary mask that identifies ice covered regions as either crevassed or not, and select all crevasses which fall in the vulnerable region as mapped by Lai et al., (2020).

For most modelled domains a very fine mesh size of 100m was used, i.e., matching or exceeding the resolution of the crevasse mask. For some of the largest ice shelves however, computational constraints required the use of a mesh resolution up to 335m. We performed a comprehensive suite of tests to ensure that all our key results are mesh independent and results of our mesh-convergence analysis is summarized in the Supplementary (Section 3). Over grounded areas in the vicinities of the GLs a resolution of maximum one ice thickness (~1000m) was applied while a larger element size was used for all elements further upstream of the GL. Elements considered to be crevassed and within the regions of vulnerability were deactivated in our perturbation experiment, by removing these elements entirely from the mesh. The correct vertically integrated ocean pressure is automatically applied at the newly formed boundaries. Several different methods were developed to determine if a given element should be deactivated or not depending on whether the element was fully within the crevassed mask, or if only some of its nodes. In all calculations presented here, we used linear triangular elements. More information regarding the tested methods and the final chosen approach is given in the Supplementary.

3 Results

3.1 Modelled changes in flux and speed

In Fig. 1 we summarize our results of the impact of crevasse activation on GL flux. In general, the introduction of crevasses leads to an increase in GL flux for all ice shelves analysed. We found that there is a substantial variability in the flux change among ice shelves, and specifically we find that, except for the two largest ice shelves (Filchner-Ronne and Ross), the resulting perturbation in flux is on the order of a few Gt/yr. Note that when calculating flux perturbations, we multiply the resulting velocity perturbation $\boldsymbol{\Delta v}$ with the ice thickness ($\boldsymbol{h}$) and ice density ($\boldsymbol{\rho}$) and then perform a line integration along all GLs of a given catchment basin and divide by the density of water to arrive at a volume of water equivalent per annum. This is the instantaneous response, and in a transient simulation the amplitude of this response is expected to reduce over time, if GLs are in a stable configuration.

Compared to the currently observed GL fluxes, the modelled changes in ice flux are, in some cases, large. For example, for the Ross and Filchner & Ronne Ice Shelves we find a 43% and 155% increase in flux, respectively. For the Amery and Getz Ice Shelves we find a 21% increase, and 32% increase for the Totten Ice Shelf. However, relative to the impact of a complete disintegration of these ice shelves, the modelled flux-changes due to crevasse activation are low. Fig. 2a displays the flux-changes resulting from crevasse activation as a function of flux-changes due to ice shelf disintegration. Results of this analysis show values of $\leq 1\%$ for most ice shelves, with slightly higher values for the Filchner & Ronne and Pine Island Ice Shelves (2%) and higher values for the Totten, Getz and Brunt Ice Shelves (4%, 5% and 17% respectively).

The total sea level contribution due to ice shelf loss was found to be orders of magnitude greater (84.4 mm/yr) than that of crevasse activation (1.45 mm/yr). This was the case for each basin studied, with the largest and most confined ice shelves contributing the greatest to sea level rise for both processes (i.e., ice shelf loss and fully vertically propagated crevasses; Figure 2b-c).

The impact of crevasse activation on GL flux is likely to be dependent on distance from the GL (Fürst et al., 2016; Reese et al., 2018a). To better asses how different ice-shelf areas contribute to modelled GL fluxes, we limited crevasse activation to ice-shelf areas within a given threshold distance from the nearest GL. For each threshold value, we modelled the activation of all identified surface crevasses in Lai et al (2020), as well as only those within the "vulnerable" areas as estimated by Lai et al (2020). The results are summarized in Figs 3 and 4.

For the two major ice shelves, Filcher-Ronne and Ross, the total modelled impact of crevasse activation over all vulnerable areas is shown in Fig. 3. The change in flux for each catchment area is displayed as red circles with areas proportional to the resulting flux perturbations. When restricting crevasse activation to regions within a given distance downstream from the grounding line, the modelled flux perturbations are always smaller than this total value. As Fig. 3 shows, most of the impact on GL flux stems from the area within the first tens of km from the major grounding line. For example, for the Filchner Ronne Ice Shelf, about 89.7% of the total flux perturbation is already produced through crevasse activation over the first 40km downstream of the major grounding line.

Modelled changes in GL ice flux, as a function of the distance threshold value, are shown in Fig. 4 for selected ice shelves. For each threshold value, all observed surface crevasses where activated. As the figure shows, generally, most of the impact is due to crevasses within the first 20 to 30km downstream of the grounding lines. In all cases more than 95% of the total flux perturbation is produced within the first 40 km. Thus, crevasses about 40km downstream of main grounding lines, are effectively passive and activation of those crevasses has negligible impact on upstream grounded flow.

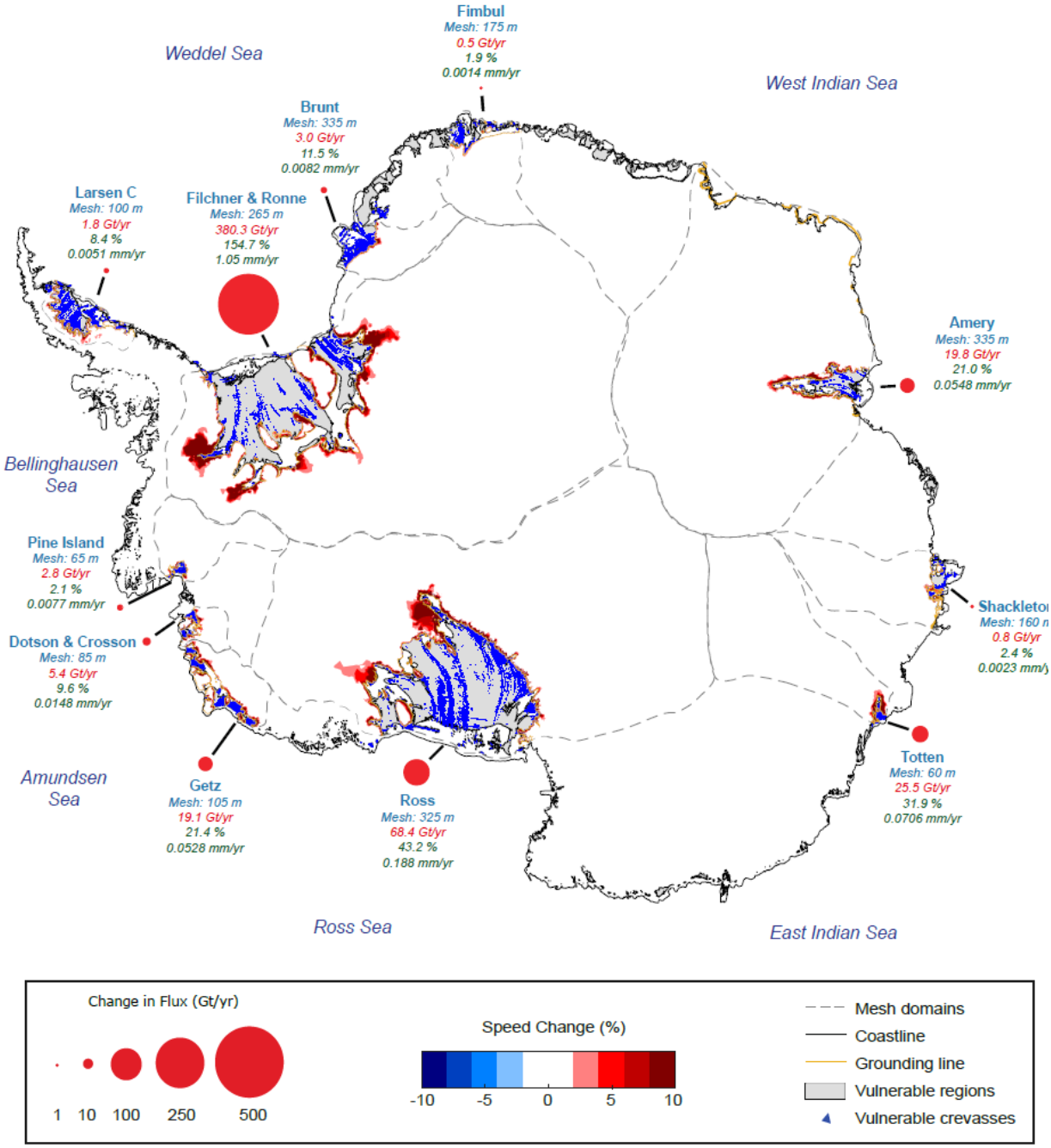

Figure 1 Modelled change in grounding-line ice flux (Gt/yr) due to crevasse activation of all identified surface crevasses within areas vulnerable to activation as mapped by Lai et al. 2020. Identified surface crevasses are shown as blue triangles, and vulnerable areas in grey. Change in flux is represented with red circles. Percentage numbers (green) show the change in flux with respect to currently observed flux. The equivalent sea level contribution for each sector is given in mm/yr (green) and change in upstream speed (%) is plotted based on the blue-white-red colourbar. Mesh boundaries (grey dashed lines), the GL (yellow lines), and the coastline (black line) are also shown.

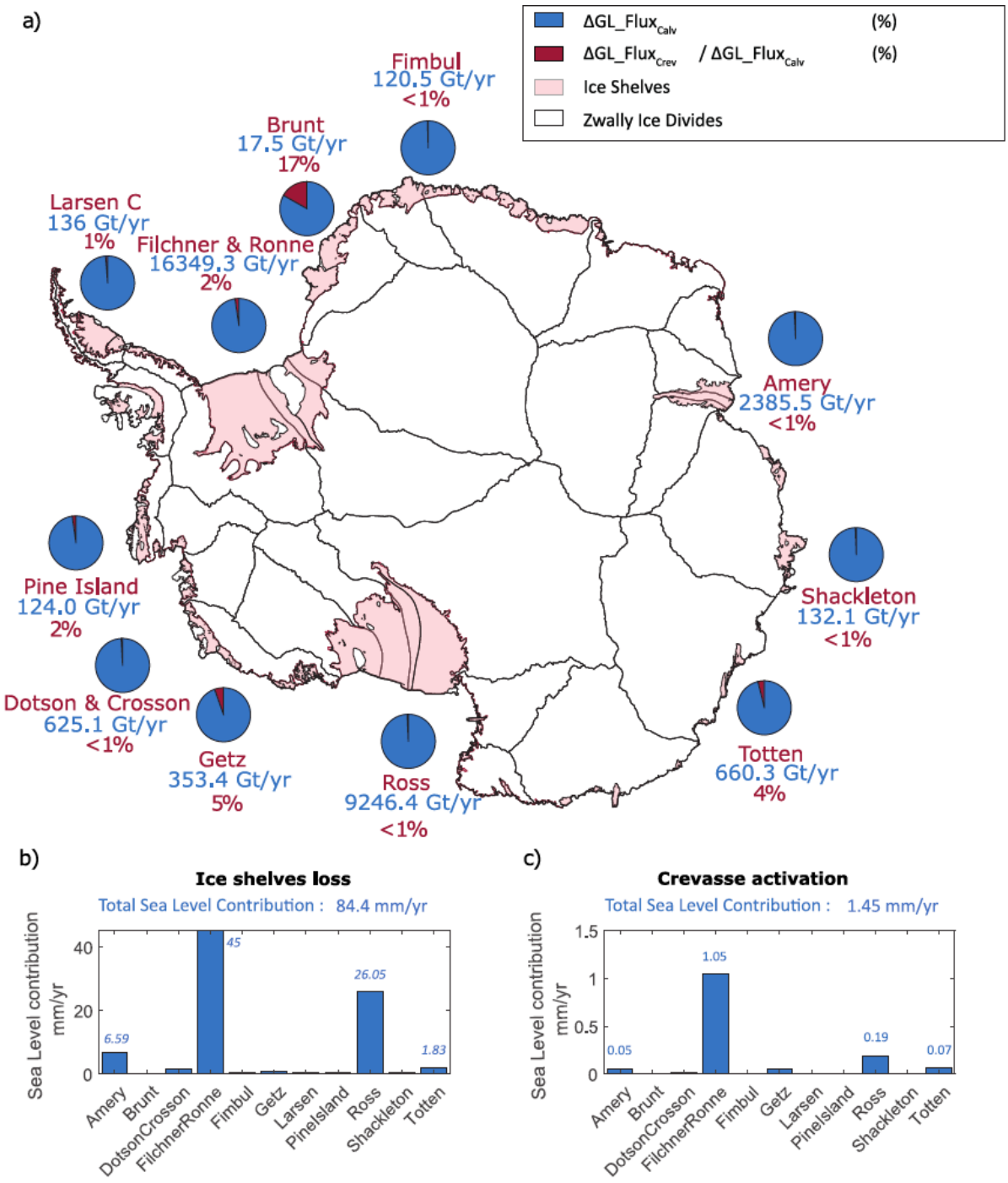

Figure 2 Modelled grounding-line flux changes. Panel a) shows modelled flux changes for each ice shelf due to ice shelf loss (text in blue), and the relative flux changes due to crevasses activation as percentage of modelled flux changes due to ice shelf loss. The resulting sea level contribution is shown in the two lower subpanels for ice shelf loss b) and crevasses activation c).

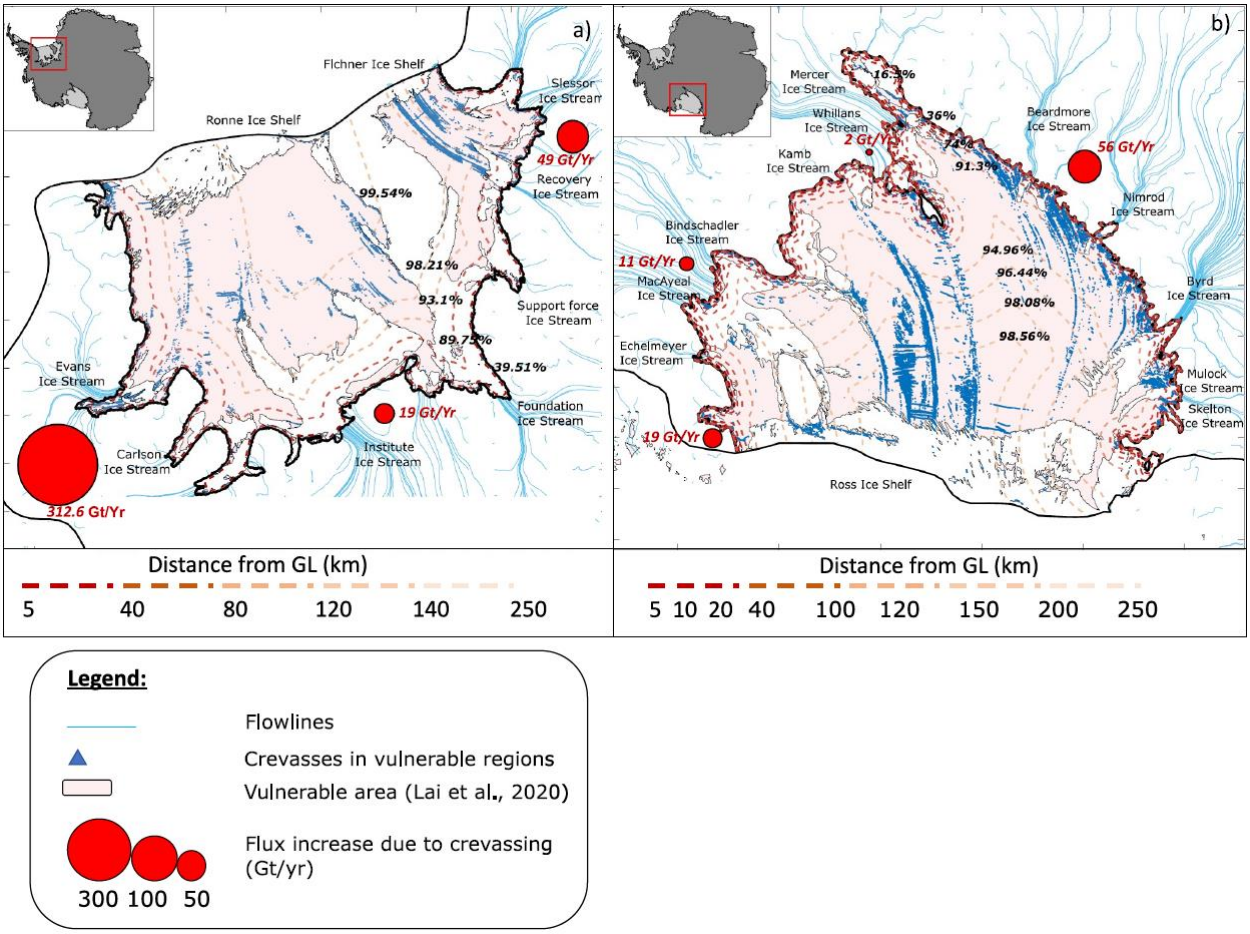

Figure 3 a) and b) Flux response for the Filchner-Ronne and Ross ice shelves due to crevasse activation within vulnerable regions of the ice shelf (following the vulnerability map of Lai et al., 2020). Red dots show modelled flux change in Gt/yr for each catchment area as defined by Zwally et al., 2012. Dashed lines, ranging from dark to pale red, define regions at different distances downstream from the main GL (km). Numbers in black displayed on top of dashed lines represent the percentages-contribution of the total flux change (the red dots) coming from crevasses activated within the region between the main GL and the dashed lines. Flowlines of ice streams are showed as pale blue lines.

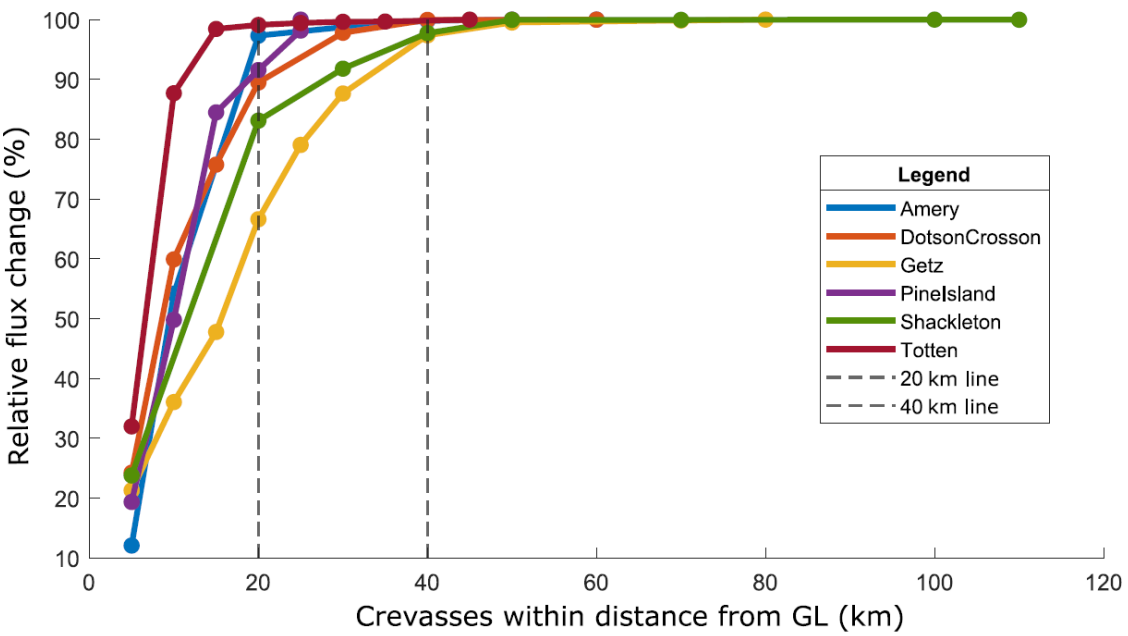

Figure 4 Relationship between crevasses located within areas of increasing distance from the main GL and the relative cumulative flux change occurring across the GL (%). This analysis was performed for all crevasses, independently from where they lie (vulnerable regions, ice front area, etc). All ice shelves' simulations show crevasses located within areas that are closer to the main GL to have a higher contribution in ice flux changes, compared to crevasses further downstream. Little or no impact is modelled for crevasses located in passive areas or close to the ice front.

Discussion

Surface and basal crevasses impact the structural integrity of ice shelves and affect the buttressing stresses that ice shelves provide to upstream grounded ice. At present, no study has quantified the effect of "instant" crevasse activation on the major ice shelves of Antarctica, and its impact in terms of upstream flux changes and sea level rise. In this study, we have explored an extreme scenario in which all currently mapped crevasses located in vulnerable ice shelf regions collectively propagate through the entire ice shelves thicknesses. We have quantified their effect on GL flux both relative to the currently observed GL flux and compared to the modelled flux perturbation following a removal of all floating ice mass.

We find calculated flux-changes to be highly variable among ice shelves studied. This directly relates to the differences in buttressing stress provided by each ice shelf in terms of their geometry, rheology, thickness, and underlaying topography (Fürst et al., 2016; Gudmundsson, 2013; Reese et al., 2018a). In our study, we find sizeable flux changes when compared with the current flux across the GL, specifically for the Filchner Ronne Ice Shelf (155% flux-increase) and for the Ross Ice Shelf (43%), and to a lesser degree for the highly confined Totten (32%) and Amery (20%) Ice Shelves.

About 90% of calculated flux-changes are caused by crevasses located within a 40 km range from the main GL. This agrees well with previous findings by Reese et al., (2018a), who concluded that buttressing was primarily generated by the sectors of the ice shelves in the immediate vicinity of the grounding lines.

By vertically propagating all crevasses simultaneously through the whole ice column, we provide an upper-limit estimate of the influence of all currently observed surface crevasses on

grounding line flux. Compared to the currently observed ice flux across the grounding lines of the Antarctic Ice Sheet, the resulting flux perturbation ranges from a few percent for Fimbul, Pine Island, and Shackleton ice shelves (see Fig 1), a few tens of percent for Totten, Getz, Amery, and Brunt ice shelves, with the highest modelled increase of 155% for the Filchner-Ronne ice shelf. However, when measured with respect to the modelled flux perturbation following a complete disintegration of all ice shelves, the changes in flux due to crevasse activation always appear rather modest. For example, for Filcher Ronne ice shelf, the flux perturbation due to crevasse activation is only 2% of the flux perturbation following the removal of the whole ice shelf. This illustrates that the structural integrity of the ice shelves is, in this sense, not particularly strongly impacted by the modelled crevasse activation. It also shows that the ice shelves still provide significant — again in this relative sense with respect to a complete ice-shelf disintegration scenario —, buttressing despite the full vertical propagation of all observed crevasses.

When comparing these results to previous continental-scale analysis, e.g. Gudmundsson et al., (2019) and Reese et al., (2018a), we find ice shelves located in the Amundsen Sea Embayment to be more sensitive to surface/basal thinning perturbations rather than to crevasse activation. An example is the small response to crevasse activation of Pine Island and Dotson and Crosson Ice Shelves. The response of Pine Island to crevasse activation is limited (0.007 mm/yr), despite having had the largest loss rate in Antarctica (58 Gt/yr, contributing 3 mm to sea level rise between 1979-2017, Rignot et al., 2019), and having a small region of passive ice (< 5%). A similar outcome was found for the Dotson and Crosson Ice Shelves, with a modelled flux-increase of < 10%, and a sea level contribution of 0.0148 mm/yr, despite Dotson having the smallest passive fraction-area among all ice shelves (1.5%, Fürst et al., 2016). Negligible changes in ice discharge were also recorded for the Larsen C and Shackleton Ice Shelf (0.0051 mm/yr, and 0.0023 mm/yr), a reassuring result since previous studies have defined these shelves as critically pre-conditioned to ice shelf disintegration in a future warming climate (Alley et al., 2018; Christie et al., 2022; Lai et al., 2020).

Our results reflect the buttressing capacity of ice shelves and highlight the sensitivity of grounding zone regions. However, while we believe it is unlikely that all currently existing crevasses would suddenly propagate through the entire ice shelves' thickness, we find that even in this scenario the effect, for the majority of ice shelves, on upstream ice discharge is low. That being said, these results provide only a snapshot of the immediate impact that ice shelf loss and activated crevasses may have on the grounded ice and represent an upper limit to this instantaneous perturbation. These effects would likely evolve through time along with crevasse development and changes in shelf geometry and stress. However, given the scope of our study, we have not explicitly modelled these transient dynamics.

Compared to the total sea level contribution of the Antarctic Ice Sheet between 1992 and 2017 (7.6 ±3.9 mm, The Imbie Team, 2018) the instant response in terms of sea level contribution (as a maximal upper limit) due to crevasse activation (1.45mm) is 5 times lower. Previous studies (Lai et al., 2020) have emphasized how warming may allow meltwater to enter vulnerable buttressing regions, enabling hydrofracture-driven ice-shelf collapse with major consequences for Antarctic mass loss and global sea-level rise. Here we show that sizeable changes do occur because of crevasse activation, although predominantly in large and confined

ice shelves, while most of the other ice shelves in Antarctica have a negligible contribution to sea level rise.

5 Conclusions

A number of previous studies have raised the possibility of crevasse propagation contributing significantly to future sea level rise. Here, we have quantified for the first time, using a numerical ice-flow model, the impact that the sudden activation of all currently observed ice shelves' crevasses would have on GL fluxes. We find that there is a positive increase in ice flux for all ice shelves studied when crevasse activation is performed, with significant variability among shelves. The largest flux-changes are measured from the highly confined ice shelves of Amery and Totten, with 20% and 32%, and to a much higher degree from the Filchner & Ronne and Ross Ice shelves, with 155% and 46% respectively. For all ice shelves, the majority of this change stems from crevasses located in grounding zone areas, where the ice is thickest, and buttressing stress highest. Overall, we find a maximal sea level contribution due to instant crevasse activation of 1.45 mm/yr, of which 1.05 mm/yr derived from the Filchner & Ronne Shelf and 0.19 mm /yr derived from the Ross Ice Shelf. However, this perturbation is small when compared to the removal of the entire ice shelf.

Acknowledgments

The authors would like to thank the editor and two anonymous reviewers for their insightful comments. Sebastian Rosier is supported by the PROPHET project, a component of the International Thwaites Glacier Collaboration (ITGC). Support from National Science Foundation (NSF: Grant 1739031) and Natural Environment Research Council (NERC: Grant NE/S006745/1). ITGC Contribution No. ITGC-098. There are no real or perceived financial conflicts of interests for any author.

Open Research

The source code of the Úa ice-flow model, sufficient to run the experiments in this project, is available at https://doi.org/10.5281/zenodo.3706624, (Gudmundsson, 2020). The crevasse mask product is available at: https://doi.org/10.15784/601335. Input datasets used in our experiments were the Antarctic drainage basins (Zwally et al., 2012), geometry from Bedmachine Antarctica v2 dataset (Morlighem et al., 2020), 2008-2009 ice-front data from ALOS PALSAR and ENVISAT ASAR (Mouginot et al., 2017), and Landsat 8 observed velocities, Fahnestock et al., 2016.

References

Alley, K. E., Scambos, T. A., Miller, J. Z., Long, D. G., & MacFerrin, M. (2018). Quantifying vulnerability of Antarctic ice shelves to hydrofracture using microwave scattering properties. *Remote Sensing of Environment*, *210*(January), 297–306. https://doi.org/10.1016/j.rse.2018.03.025

Christie, F. D. W., Benham, T. J., Batchelor, C. L., Rack, W., Montelli, A., & Dowdeswell, J. A. (2022). Antarctic ice-shelf advance driven by anomalous atmospheric and sea-ice circulation. *Nature Geoscience*, *15*(5), 356–362. https://doi.org/10.1038/s41561-022-00938-x

DeConto, R. M., & Pollard, D. (2016). Contribution of Antarctica to past and future sea-level rise. *Nature*, *531*(7596), 591–597. https://doi.org/10.1038/nature17145

Fahnestock, M., Scambos, T., Moon, T., Gardner, A., Haran, T., & Klinger, M. (2016). Rapid large-area mapping of ice flow using Landsat 8. *Remote Sensing of Environment*, *185*, 84–94. https://doi.org/10.1016/j.rse.2015.11.023

Fürst, J. J., Durand, G., Gillet-Chaulet, F., Tavard, L., Rankl, M., Braun, M., & Gagliardini, O. (2016). The safety band of Antarctic ice shelves. *Nature Climate Change*, *6*(5), 479–482. https://doi.org/10.1038/nclimate2912

Gudmundsson, G. H. (2013). Ice-shelf buttressing and the stability of marine ice sheets. *Cryosphere*, *7*(2), 647–655. https://doi.org/10.5194/tc-7-647-2013

Gudmundsson, G. H., Krug, J., Durand, G., Favier, L., & Gagliardini, O. (2012). The stability of grounding lines on retrograde slopes. *Cryosphere*, *6*(6), 1497–1505. https://doi.org/10.5194/tc-6-1497-2012

Gudmundsson, G. Hilmar, Paolo, F. S., Adusumilli, S., & Fricker, H. A. (2019). Instantaneous Antarctic ice sheet mass loss driven by thinning ice shelves. *Geophysical Research Letters*, *46*(23), 13903–13909. https://doi.org/10.1029/2019GL085027

Gudmundsson, H. (2020). GHilmarG/UaSource: Ua2019b (Version v2019b). https://doi.org/10.5281/zenodo.3706624

Hill, E., Rosier, S., Gudmundsson, H., & Collins, M. (n.d.). Quantifying uncertainty in future projections of ice loss from the Filchner- Ronne basin , Antarctica.

Hill, E. A., Hilmar Gudmundsson, G., Rachel Carr, J., & Stokes, C. R. (2018). Velocity response of Petermann Glacier, northwest Greenland, to past and future calving events. *Cryosphere*, *12*(12), 3907–3921. https://doi.org/10.5194/tc-12-3907-2018

Hill, E. A., Rosier, S. H. R., Gudmundsson, G. H., & Collins, M. (2020). Quantifying uncertainty in future projections of ice loss from the Filchner-Ronne basin , Antarctica, *770*(2014), 2020.

Lai, C. Y., Kingslake, J., Wearing, M. G., Chen, P. H. C., Gentine, P., Li, H., et al. (2020). Vulnerability of Antarctica's ice shelves to meltwater-driven fracture. *Nature*, *584*(7822), 574–578. https://doi.org/10.1038/s41586-020-2627-8

Macayeal, D. R. (1989). Large-scale ice flow over a viscous basal sediment: theory and application to ice stream B, Antarctica. *Journal of Geophysical Research*, *94*(134), 4071–4087. https://doi.org/10.1029/jb094ib04p04071

Mitcham, T., Gudmundsson, G. H., & Bamber, J. (2021). The impact of recent and future calving events on the Larsen C ice shelf. *The Cryosphere Discussions*, (April), 1–23. https://doi.org/10.5194/tc-2021-105

Morlighem, M., Rignot, E., Binder, T., Blankenship, D., Drews, R., Eagles, G., et al. (2020). Deep glacial troughs and stabilizing ridges unveiled beneath the margins of the Antarctic ice sheet. *Nature Geoscience*, *13*(2), 132–137. https://doi.org/10.1038/s41561-019-0510-8

Mouginot, J., Rignot, E., Scheuchl, B., & Millan, R. (2017). Comprehensive annual ice sheet velocity mapping using Landsat-8, Sentinel-1, and RADARSAT-2 data. *Remote Sensing*, *9*(4), 1–20. https://doi.org/10.3390/rs9040364

Reese, R., Gudmundsson, G. H., Levermann, A., & Winkelmann, R. (2018a). The far reach of ice-shelf thinning in Antarctica. *Nature Climate Change*, *8*(1), 53–57. https://doi.org/10.1038/s41558-017-0020-x

Rignot, E., Mouginot, J., Scheuchl, B., Van Den Broeke, M., Van Wessem, M. J., & Morlighem, M. (2019). Four decades of Antarctic ice sheet mass balance from 1979–2017. *Proceedings of the National Academy of Sciences of the United States of America*, *116*(4), 1095–1103. https://doi.org/10.1073/pnas.1812883116

Rosier, S. H. R., & Gudmundsson, G. H. (2018). Tidal bending of ice shelves as a mechanism

for large-scale temporal variations in ice flow. *Cryosphere*, *12*(5), 1699–1713. https://doi.org/10.5194/tc-12-1699-2018

Sun, S., Pattyn, F., Simon, E. G., Albrecht, T., Cornford, S., Calov, R., et al. (2020). Antarctic ice sheet response to sudden and sustained ice-shelf collapse (ABUMIP). *Journal of Glaciology*, *66*(260), 891–904. https://doi.org/10.1017/jog.2020.67

Team, T. I. (2018). Mass balance of the Antarctic ice sheet. *Philosophical Transactions of the Royal Society A: Mathematical, Physical and Engineering Sciences*, *364*(1844), 1627–1635. https://doi.org/10.1098/rsta.2006.1792

Trusel, L. D., Frey, K. E., Das, S. B., Karnauskas, K. B., Kuipers Munneke, P., Van Meijgaard, E., & Van Den Broeke, M. R. (2015). Divergent trajectories of Antarctic surface melt under two twenty-first-century climate scenarios. *Nature Geoscience*, *8*(12), 927–932. https://doi.org/10.1038/ngeo2563

Zwally, H. Jay Giovinetto, M.B., Beckley, M.A. & Saba, J. L. (2012). Antarctic and Greenland Drainage Systems | Earth. Retrieved July 6, 2022, from https://earth.gsfc.nasa.gov/cryo/data/polar-altimetry/antarctic-and-greenland-drainage-systems